Article

Near-complete depolymerization of polyesters with nano-dispersed enzymes

https://doi.org/10.1038/s41586-021-03408-3

Received: 14 October 2020

Accepted: 1 March 2021

Published online: 21 April 2021

Check for updates

Christopher DelRe[1,2], Yufeng Jiang[1,2], Philjun Kang[3], Junpyo Kwon[2,4], Aaron Hall[1], Ivan Jayapurna[1], Zhiyuan Ruan[1], Le Ma[1,2], Kyle Zolkin[1], Tim Li[1], Corinne D. Scown[5], Robert O. Ritchie[1,2,4], Thomas P. Russell[2,6] & Ting Xu[1,2,3] ✉

Successfully interfacing enzymes and biomachinery with polymers affords on-demand modification and/or programmable degradation during the manufacture, utilization and disposal of plastics, but requires controlled biocatalysis in solid matrices with macromolecular substrates[1–7]. Embedding enzyme microparticles speeds up polyester degradation, but compromises host properties and unintentionally accelerates the formation of microplastics with partial polymer degradation[6,8,9]. Here we show that by nanoscopically dispersing enzymes with deep active sites, semi-crystalline polyesters can be degraded primarily via chain-end-mediated processive depolymerization with programmable latency and material integrity, akin to polyadenylation-induced messenger RNA decay[10]. It is also feasible to achieve processivity with enzymes that have surface-exposed active sites by engineering enzyme–protectant–polymer complexes. Poly(caprolactone) and poly(lactic acid) containing less than 2 weight per cent enzymes are depolymerized in days, with up to 98 per cent polymer-to-small-molecule conversion in standard soil composts and household tap water, completely eliminating current needs to separate and landfill their products in compost facilities. Furthermore, oxidases embedded in polyolefins retain their activities. However, hydrocarbon polymers do not closely associate with enzymes, as their polyester counterparts do, and the reactive radicals that are generated cannot chemically modify the macromolecular host. This study provides molecular guidance towards enzyme–polymer pairing and the selection of enzyme protectants to modulate substrate selectivity and optimize biocatalytic pathways. The results also highlight the need for in-depth research in solid-state enzymology, especially in multi-step enzymatic cascades, to tackle chemically dormant substrates without creating secondary environmental contamination and/or biosafety concerns.

We envy nature's ability to program complex processes to achieve system-wide, long-term sustainability[11–14]. The key bottleneck is molecularly interfacing bio-elements with synthetic counterparts and, for enzyme-based plastic modification/degradation, how to manipulate biocatalysis with macromolecules as both the reaction substrates and host matrices[2,3,8,15]. Enzymatic activity depends on the protein structure, substrate binding and reactivity at the active site[16–18] (Fig. 1). In semi-crystalline polymers, which represent the majority of plastics[13], substrate accessibility can be rate-limiting owing to the reduced mobilities of the confined enzyme[3,4,7] and polymer matrix[19] (Fig. 1a, b). When polymers have chemically labile backbones, the enzyme can either randomly bind to and cleave a long chain, or selectively bind to the chain end and catalyse depolymerization[20,21]. Random chain scission has been the more prevalent pathway[6,14], but chain-end processive depolymerization is more desirable, because it directly and near completely converts a polymer to value-added monomers[16,22]. Selective chain-end binding is challenging in solution biocatalysis[23], but may become feasible when enzymes are nanoscopically confined to coreside with the polymer chain ends. Solid-state biocatalysis requires additional considerations that, if properly chosen, are beneficial (Fig. 1c). Thermodynamically, the polymer chain conformation contributes to the entropic gain, and thus to the global driving force of depolymerization. Kinetically, local polymer chain packing affects the segmental mobility and substrate binding to initiate and continue processive depolymerization[24,25]. Protectants used to disperse the enzyme may compete for substrate binding and/or transiently modify the active sites, offering opportunities to regulate catalytic latency[5,26]. Finally, the biocatalytic mechanism and types of targeted plastics must be considered[20,21,27]. The degradation of condensation polymers, such as polyesters, may only require substrate binding. Given their rapid market growth, understanding solid-state enzymology can lead to immediate technological impact towards single-use plastics[28–30]. However, enzymatic modifications of chemically dormant molecules, such

[1]Department of Materials Science and Engineering, University of California, Berkeley, Berkeley, CA, USA. [2]Materials Sciences Division, Lawrence Berkeley National Laboratory, Berkeley, CA, USA. [3]Department of Chemistry, University of California, Berkeley, Berkeley, CA, USA. [4]Department of Mechanical Engineering, University of California, Berkeley, Berkeley, CA, USA. [5]Energy Analysis & Environmental Impacts Division, Lawrence Berkeley National Laboratory, Berkeley, CA, USA. [6]Department of Polymer Science and Engineering, University of Massachusetts, Amherst, MA, USA. ✉e-mail: tingxu@berkeley.edu

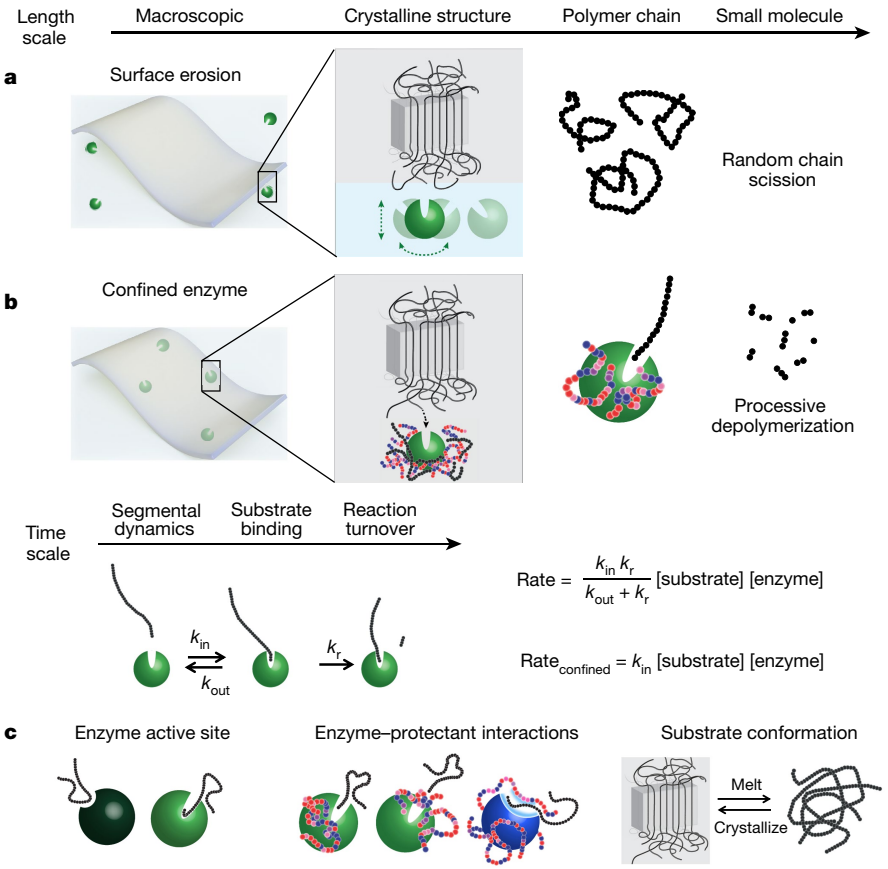

Fig. 1 | Biocatalysis with embedded enzyme for polymer degradation. **a**, **b**, Schematic illustrating two degradation pathways: plastic surface erosion with random chain scission (**a**) and chain-end binding-mediated processive depolymerization when enzymes are nanoscopically confined to co-localize with polymer chain ends in the amorphous domain (**b**). The enzyme protectants (RHPs) are used to mediate enzyme–polymer interactions for dispersion and are rendered as chains of multi-coloured beads. **b**, The reaction kinetic changes where macromolecular substrate binding becomes the rate-limiting factor with confined enzymes. The variables shown in **b** represent rate constants of a polymer chain diffusing into (k_{in}) and out of (k_{out}) the enzyme active site, and the catalytic reaction rate constant (k_r). The reaction kinetics change where macromolecular substrate binding becomes the rate-limiting factor with confined enzymes ($k_{in} << k_r$). **c**, Additional factors that modulate biocatalysis in solid states, as well as enzymatic reactions towards programmable polymer degradation. Left, a surface-exposed active site can readily bind chain segments, whereas a deep, narrow binding site prefers chain ends. Middle, the enzyme protectants (RHPs) can stabilize an enzyme, block the active site or complex with a surface-exposed binding site to implement processivity. Right, semi-crystalline polymer chain conformation affects degradation rate.

as hydrocarbons and/or polyolefins, require synchronization of multiple biocatalytic processes and are slow even under biologically optimized conditions[31]. Without knowing how microbes modify and degrade polyolefins[15,21,32,33], understanding how embedded enzymes behave will guide protein engineering and the design of hybrid bio/abio-catalysts for plastic upcycling without generating secondary environmental contamination.

By nanoscopically confining enzymes in semi-crystalline polyesters and exploiting features of enzyme active sites and enzyme–protectant interactions, we show that processive depolymerization can be enabled as the primary degradation pathway with expanded substrate selectivity. Nanoscopic dispersion of a trace amount of enzyme—for example, about 0.02 wt% lipase (<2 wt% total additives) in poly(caprolactone) (PCL) or about 1.5 wt% proteinase K (<5 wt% total additives) in poly(lactic acid) (PLA)—leads to near-complete conversion to small molecules, eliminating microplastics in a few days using household tap water and standard soil composts. The programmable degradation overcomes the incompatibility of currently used biodegradable plastics with industrial compost operations, making them viable polyolefin substitutes[28–30]. Analysis on the effects of polymer conformation and segmental cooperativity guide the thermal treatment of the polyester to spatially and temporally program degradation, while maintaining latency during processing and storage. The protectants are designed to regulate biocatalysis and stabilize enzymes during typical plastic processing. Furthermore, with embedded oxidases such as laccase and manganese peroxidase, the enzymatically generated reactive radicals cannot oxidize the host polyolefins. There is a need to understand the biocatalytic cascades to design enzyme–host interactions and to enhance the reactivity, diffusion and lifetimes of reactive species without creating biohazards.

The biodegradable plastics PCL and PLA are market-ready alternatives to many commodity plastics, offering increased production and cost reduction[34]. However, they are indifferentiable in landfills[14]. Typical residence times are not adequate to allow full breakdown even in thermophilic digesters operating at 48–60 °C (refs. [28,29]), resulting in operational challenges and a financial burden to minimize contamination in organic waste[30]. *Burkholderia cepacia* lipase (BC-lipase) and *Candida antarctica* lipase (CA-lipase) were embedded in PCL, and proteinase K was embedded in PLA, given their known hydrolysis ability in solution[15]. A previously developed four-monomer random heteropolymer (RHP) was added to nanoscopically disperse the enzymes[5,7]. RHPs adjust the segmental conformations to mediate interactions between enzymes and local microenvironments[5]. Extended Data Table 1 details the compositions of all blends.

Nano-dispersed lipase accelerates PCL degradation

At 0.02–2 wt% enzyme loading, RHP–lipase nanoclusters are uniformly distributed throughout (Fig. 2a, Extended Data Fig. 1a) and incorporated

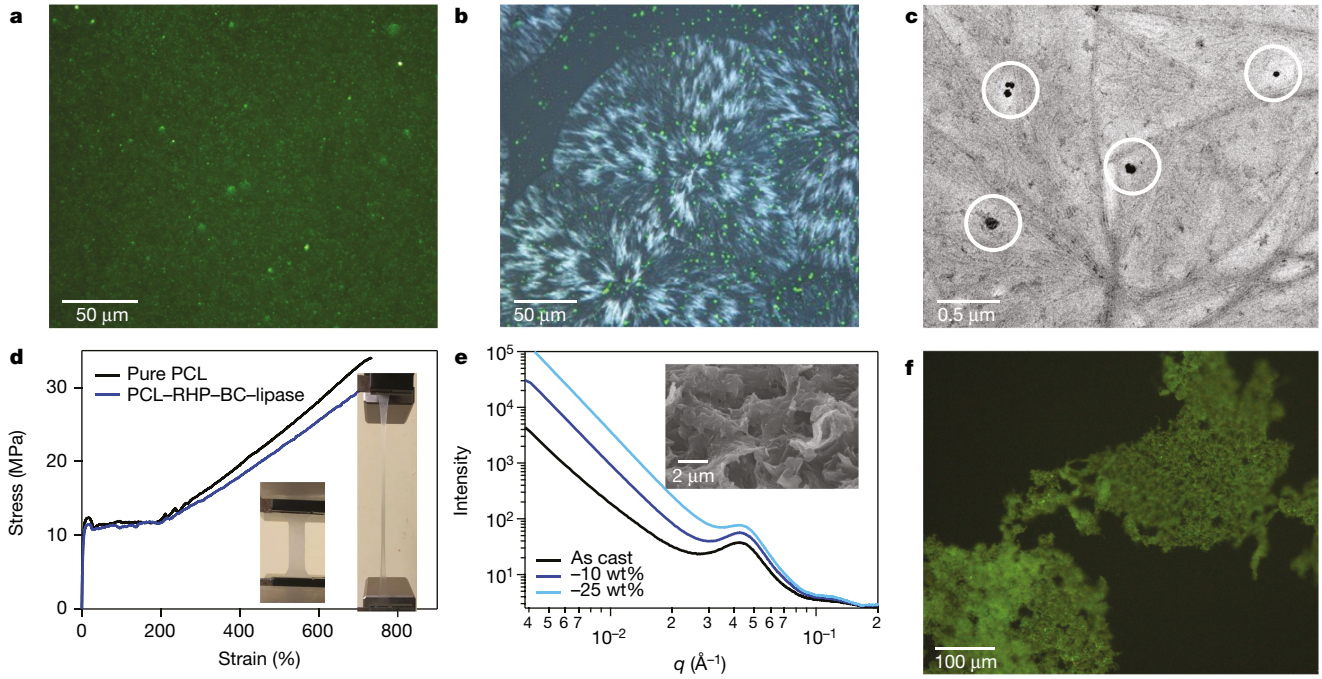

Fig. 2 | Characterization and degradation of PCL-RHP-BC-lipase. **a**, **b**, Fluorescence microscope images of a film with homogeneously distributed fluorescently labelled BC–lipase (**a**) and overlaid with a polarized optical microscope image (**b**). **c**, Transmission electron microscope (TEM) image showing incorporation of RHP–lipase within semi-crystalline spherulites. **d**, Stress–strain curve of PCL before and after RHP–BC–lipase incorporation. The inset shows a PCL–RHP–BC–lipase dog-bone sample before (left) and after (right) a tensile test. **e**, SAXS profile of PCL–RHP–BC–lipase sample with 0, 10, 25 wt% weight loss. The inset shows a cross-sectional scanning electron microscope (SEM) image from a sample with 50% weight loss. **f**, Fluorescence microscope image of microplastic particles formed after PCL–RHP–BC–lipase degraded in 40 °C buffer. Green fluorescently labelled BC–lipase remained uniformly distributed in the PCL matrix. The embedded enzymes continued to degrade PCL to achieve >95% PCL–small molecule conversion in one day.

within semi-crystalline spherulites (Fig. 2b). RHP–BC–lipase clusters, about 50 nm to around 500 nm in size, are located between bundles of PCL lamellae (Fig. 2c). Nanoscopic dispersion with minimal amounts of additives is key to retaining host properties. Small-angle X-ray scattering (SAXS) and differential scanning calorimetry (DSC) show similar PCL crystallization after lipase incorporation (Extended Data Fig. 1b, c). With lipase–RHP loadings of up to 2 wt%, there is less than 10% change in the mechanical properties of PCL (Fig. 2d). The elastic modulus and tensile strength of PCL–RHP–BC–lipase are similar to those of low-density polyethylene (LDPE). PCL containing 0.02 wt% BC–lipase degrades internally once immersed in a 40 °C buffer solution. Formation of nanoporous structure during internal degradation can be clearly seen in the cross-sectional scanning electron microscopy image, and leads to increase in scattering intensity when the scattering vector is $q < 0.04$ Å^{-1}, owing to enhanced contrast between the PCL and air (Fig. 2e). After being disintegrated into microplastic particles (Fig. 2f), fluorescently labelled BC–lipase remains encapsulated and continues to degrade the microplastics to achieve up to 98% conversion within 24 h.

The overall PCL crystallinity in PCL–RHP–BC–lipase does not change when the degradation weight loss increases from 20% to 80% (Fig. 3a). Thus, the PCL segments in both the amorphous and crystalline phases degrade, as opposed to mainly the amorphous segments, which typically occurs for random scission processes. This is consistent with the SAXS results in Fig. 2e, where the peak position associated with lamella periodicity does not change. The PCL molecular weight remains the same despite substantial weight loss (Fig. 3b). The primary degradation by-products are repolymerizable small molecules, less than 500 Da in size (Fig. 3c, Extended Data Fig. 2). Control experiments with PCL degradation via random chain scission show a wide range of high-molecular-weight oligomers. Thus, the degradation of PCL–RHP–BC–lipase should proceed via processive depolymerization.

Design of enzyme–polymer blends for processive depolymerization

When BC–lipase nanoclusters are embedded in pure PLA or a PCL–PLA blend, no PLA hydrolysis is observed, even though lipase catalyses a broad range of hydrolysis reactions[35]. However, when the host matrix is a PCL-b-PLA diblock copolymer (40-b-20 kDa), both the PCL and PLA blocks depolymerize into small molecules with a similar molar ratio as the parent copolymer (Fig. 3d). Thus, once a PCL chain end binds to the active site and is depolymerized by the BC–lipase, the PLA block can be shuttled to the active site and subsequently depolymerized. This is strikingly similar to polyadenylation-induced processive mRNA degradation[10], opening a useful route to expand substrate selection.

BC–lipase shares common traits with processive enzymes[16,23,24]. It has a deep (up to 2 nm), narrow (4.5 Å at the base) hydrophobic cleft from its surface to the catalytic triad[17], which may facilitate substrate polymer-chain sliding while preventing dissociation. Opposite to the hydrophobic binding patch are six polar residues that provide a potential driving force to pull the remaining chain forwards after hydrolysis (Fig. 3e, left). Once the chain end is bound, the BC–lipase processively catalyses the depolymerization without releasing it[23]. CA–lipase has a surface-exposed, shallow active site (about 1 nm from the surface) with no obvious residues that afford processivity (Fig. 3e, right). With random scission being the dominant pathway (Extended Data Fig. 3), PCL–RHP–CA lipase degradation stops after about 12% mass loss, and the bulk PCL crystallinity increases as degradation proceeds. Thus, the surface chemistry of the enzyme and the shape of the active site have important roles in modulating polymeric substrate binding towards preferential processive depolymerization.

Without nanoscopic confinement, BC–lipase degrades PCL via random chain scission in solution. When BC–lipase is embedded as

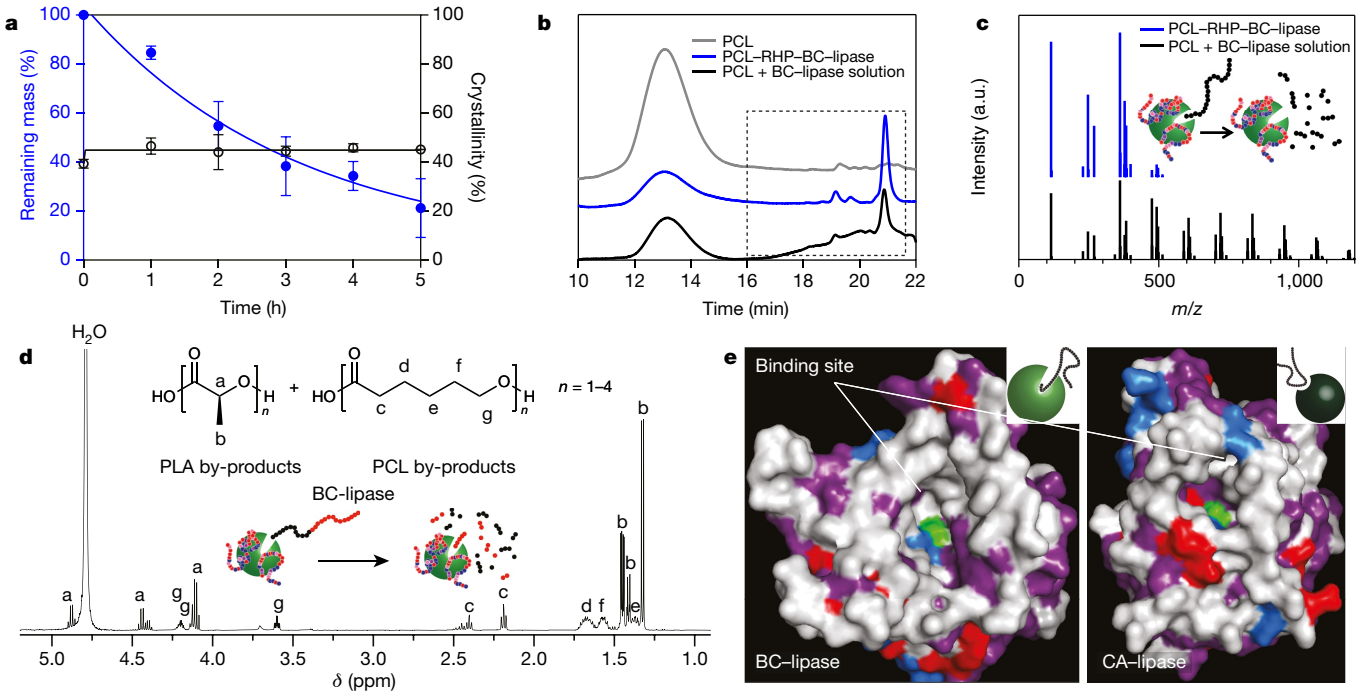

Fig. 3 | Embedded BC–lipase depolymerizes polyesters via chain end-mediated processive degradation. a, Remaining mass (closed blue circles) and per cent crystallinity (open black circles) of PCL–RHP–BC–lipase samples as a function of degradation time in 37 °C buffer (error bars represent one standard deviation; $n \geq 3$ for remaining mass, $n \geq 2$ for crystallinity). **b**, Gel permeation chromatography (GPC) of PCL samples after surface erosion and confined degradation by BC–lipase, including the remaining film and degraded by-product. **c**, Mass spectra of PCL degraded by surface erosion or by confined BC–lipase, including the remaining film and degraded by-product. The *x* axis (*m*/*z*) shows mass divided by charge, and the inset depicts processive depolymerization. **d**, Nuclear magnetic resonance (NMR) spectra of degradation by-products of PCL-b-PLA diblock copolymer when blended with RHP–BC–lipase. Both small-molecule by-products of PCL and PLA were seen in BC lipase-containing diblock matrices, whereas only PCL degradation was observed for PCL–PLA blend matrices. The *x* axis (δ) shows the chemical shift. **e**, Surface representation of BC–lipase and CA–lipase, highlighting the hydrophobic (white) substrate binding domain and the polar (purple) patch across from the binding domain; catalytic serine residue is shown in green, whereas negative and positive residues are shown in red and blue, respectively. a.u., arbitrary units.

micrometre-sized aggregates, the host degradation stops after about 40% mass loss, and leads to highly crystalline, long-lasting microplastics[6,8,9] (Extended Data Fig. 4a). Furthermore, PCL–RHP–BC–lipase undergoes negligible degradation at room temperature in buffer solution for >3 months, whereas BC–lipase in solution degrades about 30% of pure PCL in 2 days. The hindered mobilities of the embedded enzyme and PCL segments limit initial substrate binding and depolymerization.

The turnover rate for PCL depolymerization by embedded BC–lipase is about 30 s^{-1} for 0–3 h and around 12 s^{-1} after 3 h. The turnover rates of BC–lipase are about 200 s^{-1} in solution with small-molecule substrate, around 19 s^{-1} in solution with a PCL film as substrate, and about 120 s^{-1} in PCL–RHP–BC–lipase with a small-molecule substrate (Extended Data Fig. 4b). The embedded lipase shows a similar or higher apparent activity towards PCL than that in solution, where lipase has high rotational and translational freedom with higher substrate availability (that is, polymer segments as opposed to chain ends). Thus, depolymerization kinetics are mainly governed by substrate binding for embedded enzymes and benefit considerably from a chain-end-mediated processive depolymerization pathway.

Therefore, to realize chain-end-mediated processive depolymerization, the enzyme should be nanoscopically confined to co-reside with the polymer chain ends, exclude the middle segments from reaching the catalytic site, and have attractive interactions with the remaining chain end to slide the polymer chain without dissociation. With processive depolymerization, the host degrades with near-complete polymer-to-small-molecule conversion, eventually eliminating highly crystalline microplastic particles. Kinetically, the apparent degradation rate benefits from substrate shuttling, and catalytic latency can be regulated by thermal treatment and/or operation temperature.

RHPs modulate enzyme stability

RHPs assist nanoscopic dispersion of enzymes and affect the local micro-environment, substrate accessibility and possibly the degradation pathway. A model experiment at the solvent–water interface was designed in which the interfacial tension is used to monitor molecular associations of the enzyme, RHP and polymer (Extended Data Fig. 5a, b). Using pendant drop tensiometry, the toluene–water interfacial tension (γ) decreases from 36 to 27 mN m^{-1} when PCL is in toluene, to about 10 mN m^{-1} with lipase in water, and to less than 5 mN m^{-1} with only RHP in toluene. When all three components are in toluene, the interfacial tension is 27 mN m^{-1} initially, remains unchanged for a period of time, and then drops rapidly before plateauing at about 7 mN m^{-1} and remains constant. Fluorescently labelled lipase immediately concentrates at the toluene–water interface (Extended Data Fig. 5c). Taken together with the tensiometry data (Extended Data Fig. 5d), RHP–lipase complexes remain associated with PCL chains, and all three components concentrate together at the toluene–water interface. As lipase degrades PCL, the shorter chains desorb and expose the RHP–lipase complex, causing the reduction in tension. Thus, there is a coordinated interplay at the interface: PCL binds to the lipase and RHP facilitates the introduction of PCL into lipase, whereupon PCL degrades and leaves only the RHP–lipase complexes at the interface. Because the driving force required for PCL to dissociate from the lipase–RHP complex in dilute solution is higher than that in the melt, RHPs remain associated with lipase inside PCL.

The RHPs modulate the micro-environment of enzymes and provide entropic stabilization, enabling scalable processing of enzyme-embedded plastics using melt extrusion. PCL–RHP–BC–lipase

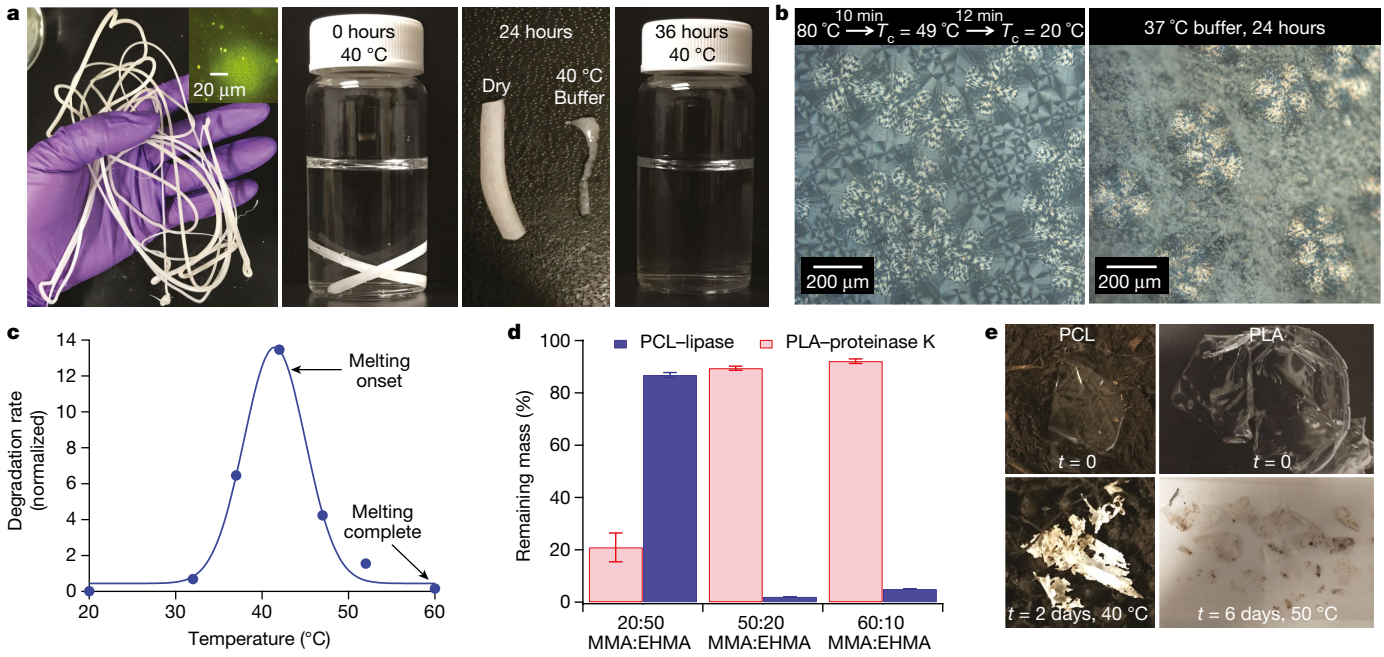

Fig. 4 | Enzyme protectants (RHPs) associate with the embedded enzyme to retain activity during melt processing and thermal treatment to program degradation. a, Melt-extruded PCL–RHP–BC–lipase filaments containing about 0.1 wt% lipase that degrades into small molecules with near-complete conversion within 36 h in 40 °C buffer. **b**, Programming of PCL–RHP–BC–lipase degradation by thermal treatment. Polarized optical imaging confirms that only regions with a low crystallization temperature are degraded after 24 h in 37 °C buffer. **c**, Programming of PCL–RHP–BC–lipase degradation by degradation temperature. The degradation rate of PCL–RHP–BC–lipase is substantially suppressed below the onset of the PCL melting temperature or in amorphous PCL melt. This ensures PCL integrity during storage and melt processing. **d**, RHPs can modulate depolymerization in PCL–BC–lipase and PLA–proteinase K. The remaining mass shown is after 1 day of immersion in buffer for PCL–BC–lipase, after 7 days for PLA-proteinase K with 20:50 MMA:EHMA RHP composition, and after 1 month for PLA–proteinase K with 50:20 and 60:10 MMA:EHMA RHP compositions ($n \geq 3$). **e**, Enzyme-containing PCL (left) and PLA (right) readily break down in ASTM standard composts.

containing about 0.1 wt% lipase was extruded at 85 °C to produce a ~1.5-mm-diameter filament, which degrades nearly completely over 36 h in buffer by the same processive depolymerization mechanism (Fig. 4a).

Programming of catalytic latency

Polymer degradation can be programmed by thermal treatments. As the BC–lipase pulls the segments in the PCL stem that spans the crystalline lamellae, the competing force is governed by multiple pair-wise interactions between chains, and degradation should not occur above a critical lamella thickness. Indeed, PCL–RHP–BC–lipase films with thicker crystalline lamellae (crystallized at 49 °C) undergo negligible degradation over 3 months in 37 °C buffer, whereas films with thinner crystalline lamellae (crystallized at 20 °C) degrade over 95% in 24 h (Extended Data Fig. 6). This dependence on lamella thickness is exploited to spatially vary degradation within the same film (Fig. 4b). Control experiments using CA–lipase show no dependence on thermal treatment or lamella thickness, as expected for the random scission pathway.

The operation temperature is another handle for programming degradation latency. There is a much lower conformational entropic penalty for a crystallized chain segment to bind to an enzyme than a completely amorphous chain[36]. The high entropic penalty for enzyme binding overtakes the effects of increased chain mobility, leading to large reductions in degradation rates at higher temperatures (>43 °C) (Fig. 4c) and eventually minimal PCL degradation in the melt state (>60 °C) despite the higher enzymatic activity against small molecule substrates (Extended Data Fig. 7). These results counter the long-standing opinion that crystallinity slows enzymatic degradation of both synthetic[18,20] and natural[24,37] polymers, and enable the application of chain-end-mediated processive depolymerization to ensure catalytic latency and polymer integrity during melt processing and long-term storage.

RHPs modulate catalytic kinetics and pathway

Proteinase K readily degrades PLA but the active site is highly surface-exposed, so that partial PLA degradation occurs with random chain scission, leaving highly crystalline microplastics behind. We hypothesize that modulating interactions between the proteinase K binding site and RHPs may create an RHP-covered active site to achieve the characteristics of processive enzymes without protein engineering. We experimentally screen RHPs guided by the analysis of RHP segmental hydrophobicity[38] (Extended Data Fig. 8) and the surface chemistry of a proteinase K active site (Extended Data Fig. 9a). The compositions of two hydrophilic monomers, oligo(ethylene glycol methyl ether methacrylate) (OEGMA) at 25% and sulfopropyl methacrylate potassium salt (SPMA) at 5%, are kept constant and the compositions of two hydrophobic monomers, methyl methacrylate (MMA) and ethyl hexyl methacrylate (EHMA) are varied. When the RHP with 20:50 MMA:EHMA composition is used, PLA depolymerizes into small-molecule by-products readily, without any observable change in the molecular weight or formation of intermediate molecular weight by-products (Fig. 4d, red; Extended Data Fig. 9b). Tensiometry studies at the DCM–water interface confirm proteinase K–RHP complexation and the PLA binding at the early stage of complexation (Extended Data Fig. 9c). This suggests that the RHP binds to the enzyme surface to facilitate processivity by forming a hybrid 'binding pocket' with proteinase K and shuttles in the PLA chains. However, when RHPs with compositions of 50:20 and 60:10 MMA:EHMA are used, minimal PLA depolymerization is observed with only about 10% mass loss after 1 month in buffer despite high activity against a small-molecule ester. Similarly, the RHP composition also affects the depolymerization rate of PCL (Fig. 4d, blue). Thus, besides being enzyme protectants, RHPs can be designed to regulate substrate binding and active-site availability, a useful handle

to guide enzyme active-site engineering[39]. Experimentally, when 1.5 wt% of proteinase K with 3 wt% of RHPs are embedded, about 80 wt% PLA depolymerizes in 1 week in buffer at 37 °C. Both enzyme-containing PCL and PLA show accelerated depolymerization in industrial soil composts (Fig. 4e), and films clearly disintegrate in a few days within the operating temperature range of industrial compost facilities (2 days at 40 °C for PCL and 6 days at 50 °C for PLA).

The hydrocarbon substrate is inaccessible to embedded oxidases

Besides synthetic catalysts[22], biocatalysis of hydrocarbons is highly desirable owing to its known efficiency, selectivity and programmability[31]. However, polyolefin degradation has mainly been reported using microbes, as opposed to enzymes[21]. Polyolefin degradation is often initiated by side-chain modification, such as oxidation. To probe the bottlenecks, manganese peroxidase from white rot fungus and laccase from Trametes versicolor are embedded either in polyethylene or polystyrene with and without mediators (Tween 80 for manganese peroxidase and hydroxybenzotriazole for laccase). After two weeks in malonate buffer at 30 °C or 60 °C, no changes are observed for any enzyme–polyolefin blends by infrared spectroscopy and GPC. For biosafety, these results are reassuring and expected with the known longevity of plastic wastes. However, both enzymes remain highly active inside the plastics according to colorimetric assays, confirming formation of diffusive reactive radicals (Extended Data Fig. 9d). Tensiometry studies confirm complexation between RHPs and both enzymes, but not between enzymes and polyolefins (Extended Data Fig. 9e). The results suggest that the radicals generated cannot reach the polyolefin substrates, most probably because of limited diffusion, insufficient lifetime of reactive radicals, and the energy barrier to cross the interfacial layer between the enzyme and hydrocarbon chains.

Once nanoscopically confined, enzyme behaviour in a solid matrix varies considerably. Understanding enzymes in plastics not only gives new insights into solid-state enzymology with a macromolecular substrate, but also enables fabrication of functional plastics with programmable life cycles compatible with plastic melt processing. Considering recent developments in synthetic biology and biodegradable plastic production[14,34,39], modulating biocatalysis of embedded enzymes can lead to molecular control over reaction pathway, kinetics, latency and production of high-value by-products. However, there is great need to understand the reaction mechanism of embedded enzymes, especially for multi-step enzymatic cascades, and how to facilitate substrate accessibility in solid-state enzymology. These insights are paramount to avoiding turning these extensively used plastics into environmental biohazards.

Online content

Any methods, additional references, Nature Research reporting summaries, source data, extended data, supplementary information, acknowledgements, peer review information; details of author contributions and competing interests; and statements of data and code availability are available at https://doi.org/10.1038/s41586-021-03408-3.

1. Tokiwa, Y. & Suzuki, T. Hydrolysis of polyesters by lipases. *Nature* **270**, 76–78 (1977).
2. Tournier, V. et al. An engineered PET depolymerase to break down and recycle plastic bottles. *Nature* **580**, 216–219 (2020).
3. Kuchler, A., Yoshimoto, M., Luginbuhl, S., Mavelli, F. & Walde, P. Enzymatic reactions in confined environments. *Nat. Nanotechnol.* **11**, 409–420 (2016).
4. Yang, Z. et al. Activity and stability of enzymes incorporated into acrylic polymers. *J. Am. Chem. Soc.* **117**, 4843–4850 (1995).
5. Panganiban, B. et al. Random heteropolymers preserve protein function in foreign environments. *Science* **359**, 1239–1243 (2018).
6. Ganesh, M., Dave, R. N., L'Amoreaux, W. & Gross, R. A. Embedded enzymatic biomaterial degradation. *Macromolecules* **42**, 6836–6839 (2009).
7. DelRe, C. et al. Reusable enzymatic fiber mats for neurotoxin remediation in water. *ACS Appl. Mater. Inter.* **10**, 44216–44220 (2018).
8. Khan, I., Nagarjuna, R., Dutta, J. R. & Ganesan, R. Enzyme-embedded degradation of poly(epsilon-caprolactone) using lipase-derived from probiotic *Lactobacillus plantarum*. *ACS Omega* **4**, 2844–2852 (2019).
9. Huang, Q. Y., Hiyama, M., Kabe, T., Kimura, S. & Iwata, T. Enzymatic self-biodegradation of poly(L-lactic acid) films by embedded heat-treated and immobilized proteinase K. *Biomacromolecules* **21**, 3301–3307 (2020).
10. Xu, F. F. & Cohen, S. N. RNA degradation in *Escherichia coli* regulated by 3′ adenylation and 5′ phosphorylatian. *Nature* **374**, 180–183 (1995).
11. Wei, R. et al. Possibilities and limitations of biotechnological plastic degradation and recycling. *Nat. Catal.* **3**, 867–871 (2020).
12. Ivleva, N. P., Wiesheu, A. C. & Niessner, R. Microplastic in aquatic ecosystems. *Angew. Chem. Int. Ed.* **56**, 1720–1739 (2017).
13. Jambeck, J. R. et al. Plastic waste inputs from land into the ocean. *Science* **347**, 768–771 (2015).
14. Haider, T. P., Volker, C., Kramm, J., Landfester, K. & Wurm, F. R. Plastics of the future? The impact of biodegradable polymers on the environment and on society. *Angew. Chem. Int. Ed.* **58**, 50–62 (2019).
15. Roohi, et al. Microbial enzymatic degradation of biodegradable plastics. *Curr. Pharm. Biotechnol.* **18**, 429–440 (2017).
16. Breyer, W. A. & Matthews, B. W. Structure of *Escherichia coli* exonuclease I suggests how processivity is achieved. *Nat. Struct. Biol.* **7**, 1125–1128 (2000).
17. Pleiss, J., Fischer, M. & Schmid, R. D. Anatomy of lipase binding sites: the scissile fatty acid binding site. *Chem. Phys. Lipids* **93**, 67–80 (1998).
18. Li, S. M. & McCarthy, S. Influence of crystallinity and stereochemistry on the enzymatic degradation of poly(lactide)s. *Macromolecules* **32**, 4454–4456 (1999).
19. Flory, P. J. & Yoon, D. Y. Molecular morphology in semi-crystalline polymers. *Nature* **272**, 226–229 (1978).
20. Tokiwa, Y., Calabia, B. P., Ugwu, C. U. & Aiba, S. Biodegradability of plastics. *Int. J. Mol. Sci.* **10**, 3722–3742 (2009).
21. Ru, J. K., Huo, Y. X. & Yang, Y. Microbial degradation and valorization of plastic wastes. *Front Microbiol* **11**, 442, (2020).
22. Tennakoon, A. et al. Catalytic upcycling of high-density polyethylene via a processive mechanism. *Nat. Catal.* **3**, 893–901 (2020).
23. Horn, S. J. et al. Costs and benefits of processivity in enzymatic degradation of recalcitrant polysaccharides. *Proc. Natl Acad. Sci. USA* **103**, 18089–18094 (2006).
24. Beckham, G. T. et al. Molecular-level origins of biomass recalcitrance: decrystallization free energies for four common cellulose polymorphs. *J. Phys. Chem. B* **115**, 4118–4127 (2011).
25. Payne, C. M., Himmel, M. E., Crowley, M. F. & Beckham, G. T. Decrystallization of oligosaccharides from the cellulose Iβ surface with molecular simulation. *J. Phys. Chem. Lett.* **2**, 1546–1550 (2011).
26. Klibanov, A. M. Improving enzymes by using them in organic solvents. *Nature* **409**, 241–246 (2001).
27. Christensen, P. R., Scheuermann, A. M., Loeffler, K. E. & Helms, B. A. Closed-loop recycling of plastics enabled by dynamic covalent diketoenamine bonds. *Nat. Chem.* **11**, 442–448 (2019).
28. Satchwell, A. J. et al. Accelerating the deployment of anaerobic digestion to meet zero waste goals. *Environ. Sci. Technol.* **52**, 13663–13669 (2018).
29. Hobbs, S. R., Parameswaran, P., Astmann, B., Devkota, J. P. & Landis, A. E. Anaerobic codigestion of food waste and polylactic acid: effect of pretreatment on methane yield and solid reduction. *Adv. Mater. Sci. Eng.* **2019**, 4715904 (2019).
30. Nordahl, S. L. et al. Life-Cycle Greenhouse Gas Emissions and Human Health Trade-Offs of Organic Waste Management Strategies. *Environ. Sci. Technol.* **54**, 9200–9209 (2020).
31. Radi, R. Oxygen radicals, nitric oxide, and peroxynitrite: redox pathways in molecular medicine. *Proc. Natl Acad. Sci. USA* **115**, 5839–5848 (2018).
32. Iiyoshi, Y., Tsutsumi, Y. & Nishida, T. Polyethylene degradation by lignin-degrading fungi and malaganese peroxidase. *J. Wood Sci.* **44**, 222–229 (1998).
33. Yang, J., Yang, Y., Wu, W. M., Zhao, J. & Jiang, L. Evidence of polyethylene biodegradation by bacterial strains from the guts of plastic-eating waxworms. *Environ. Sci. Technol.* **48**, 13776–13784 (2014).
34. Schneiderman, D. K. & Hillmyer, M. A. There is a great future in sustainable polymers. *Macromolecules* **50**, 3733–3749 (2017).
35. Liu, L. J., Li, S. M., Garreau, H. & Vert, M. Selective enzymatic degradations of poly(L-lactide) and poly(epsilon-caprolactone) blend films. *Biomacromolecules* **1**, 350–359 (2000).
36. Varma-Nair, M., Pan, R. & Wunderlich, B. Heat capacities and entropies of linear, aliphatic polyesters. *J. Polym. Sci. Pol. Phys.* **29**, 1107–1115 (1991).
37. Hall, M., Bansal, P., Lee, J. H., Realff, M. J. & Bommarius, A. S. Cellulose crystallinity – a key predictor of the enzymatic hydrolysis rate. *FEBS J.* **277**, 1571–1582 (2010).
38. Jiang, T. et al. Single-chain heteropolymers transport protons selectively and rapidly. *Nature* **577**, 216–220 (2020).
39. Arnold, F. H. Directed evolution: bringing new chemistry to life. *Angew. Chem. Int. Ed.* **57**, 4143–4148 (2018).

Methods

Embedding random heteropolymer enzymes in polyesters

Amano PS lipase from *Burkholderia cepacia* (BC–lipase), *Candida antarctica* lipase B (CA–lipase) and proteinase K from *Tritirachium album* were purchased from Sigma Aldrich. The BC–enzyme solution was purified following established procedure[40]. Proteinase K was purified by using a 10,000 g mol^{-1} molecular-weight cutoff filter by spinning in a centrifuge at 6,000 relative centrifugal force (rcf) for three cycles. The concentration of the purified lipase and proteinase K stock solution was determined using ultraviolet–visible absorbance at 280 nm. Detailed information for all samples is listed in Extended Data Table 1.

The RHP (70 kDa; polydispersity, PDI = 1.55) was synthesized[5]. The monomer molar composition used, unless otherwise specified, was 50% MMA, 20% EHMA, 25% OEGMA (number-average molecular weight, M_n = 500 g mol^{-1}) and 5% SPMA. The RHP is defined as MMA:EHMA:OEGMA:SPMA = 0.5:0.2:0.25:0.05. Two RHP variants were used to perform experiments described in Fig. 4d with composition of MMA:EHMA:OEGMA:SPMA = 0.6:0.1:0.25:0.05 and MMA:EHMA:OEGMA:SPMA = 0.2:0.5:0.25:0.05.

RHP and enzymes were mixed in aqueous solution, flash-frozen in liquid nitrogen, and lyophilized overnight. The dried RHP–enzyme mixture was resuspended directly in the specified polymer solutions or melts. RHP was mixed with purified BC–lipase in a mass ratio of 80:1 (total polymer matrix mass, 98.6%). For commercial BC–lipase and CA–lipase blends, the RHP-to-blend weight ratio was kept at 2:1 (total polymer matrix mass, 95.5%). For proteinase K in PLA, a 2:1 RHP:enzyme ratio was used (total polymer matrix mass, 95.5%).

PCL (80 kDa) and PLA (85–160 kDa) were purchased from Sigma Aldrich and used without further purification. To prepare solution-cast films, PCL (or PLA) was dissolved in toluene (or dichloromethane) at 4 wt% concentration and stirred for at least 4 h to ensure complete dissolution. The dried RHP–enzyme complexes were resuspended at room temperature directly in the polymer solution at the specified enzyme concentration. Mixtures were vortexed for ~5 min before being cast directly on a glass plate. PCL films were air-dried and PLA films were dried under a glass dish to prevent rapid solvent evaporation, given the volatility of dichloromethane.

To probe enzyme distribution, lipase was fluorescently labelled. NHS–fluorescein (5/6-carboxyfluorescein succinimidyl ester) was used to label lipase by following the manufacturer's procedure; excess dye was removed using a centrifuge filter. A U-MWBS3 mirror unit with 460–490 nm excitation wavelength was used to take the fluorescence microscopy images. TEM images were taken on a JEOL 1200 microscope at 120 kV accelerating voltage. Vapour from a 0.5 wt% ruthenium tetroxide solution was used to stain the RHP–lipase and the amorphous PCL domains.

Characterization of as-cast plastics

Dynamic light scattering (DLS) was used to obtain the complex's particle size in toluene. The crystallinity and mechanical properties of enzyme-embedded polyesters were probed via differential scanning calorimetry (DSC) and tensile testing, respectively. For DSC, ~5-mg PCL films were pressed into aluminium pans and heated from 25 °C to 70 °C at a scan rate of 2 °C min^{-1}. To quantify the per cent crystallinity, the sample's enthalpy of melting was normalized by 151.7 J g^{-1}, the enthalpy of melting for 100% crystalline PCL[41]. For uniaxial tensile tests, PCL solutions were cast directly in custom-designed Teflon moulds with standard dog-bone shapes. For SAXS studies, ~300-μm-thick films were cast in Teflon beakers. Samples were vacuum-dried after degradation for 16 h before running SAXS at beamline 7.3.3 at the Advanced Light Source (ALS) in Berkeley, USA. X-rays with 1.24 Å wavelength and 2 s exposure times were used. The scattered-X-ray intensity distribution was detected using a high-speed Pilatus 2M detector. Images were plotted as intensity (I) versus q, where $q = (4\pi/\lambda)\sin\theta$, where λ is the wavelength of the incident X-ray beam and 2θ is the scattering angle. The sector-average profiles of SAXS patterns were extracted using Igor Pro with the Nika package. The same SAXS method was used to analyse the nanoporous structure of samples at different time points of the degradation process, as shown in Fig. 2e. To obtain the cross-sectional SEM image shown in the inset to Fig. 2e, the degraded film was rinsed and fractured in liquid nitrogen. The film was then mounted on an SEM stub and sputter-coated with platinum before imaging.

Characterization of enzyme-embedded PCL degradation

Degradation was carried out in sodium phosphate buffer (25 mM, pH 7.2) at the specified temperature. Mass loss was determined by drying the remaining film and measuring the mass on a balance. After 24 h, mass loss was estimated by integrating GPC peaks. The microplastic experiment shown in Fig. 2f was run with a ~5-mg PCL–RHP–BC–lipase film (0.02 wt% enzyme) in 3 ml of buffer at 40 °C. The same experiment was run with fluorescently labelled enzyme.

At each time point from 0–5 h, the remaining PCL–RHP–BC–lipase films were dried and analysed via DSC to determine crystallinity. To analyse degradation by-products, vials were lyophilized overnight before resuspending in the proper solvent for GPC or LC-MS. GPC measurements were run using a total concentration of 2 mg ml^{-1} of remaining film and by-product in THF. 20 μl of solution was injected into an Agilent PolyPore 7.5×300 mm column; the GPC spectrum for BC–lipase in solution was normalized to the solvent front. Liquid chromatography–mass spectrometry (LC-MS) measurements were obtained by resuspending degradation supernatant in acetonitrile/water (67/33 vol%) using an Agilent InfinityLab EC-C18, 2.7-μm column. Control experiments for surface erosion were run with ~0.15 mg ml^{-1} total BC–lipase blend concentration. The mass spectrum shown in Fig. 3c is a combination of the major peaks seen in the chromatogram (Extended Data Fig. 2). The by-products were repolymerized as proof of concept using a previously reported method[42], after recovering the degraded PCL by-product from enzyme and buffer salts via phase extraction and filtration.

Enzyme active site affects degradation by confined enzymes

RHP–BC–lipase was embedded in a PCL-b-PLA diblock copolymer blended with pure PLA for the testing, because the diblock on its own was too brittle to form a free-standing film after drying. The film was cast from a solution of 9 wt% PCL-b-PLA (purchased from Polymer Source) and 4 wt% pure PLA in dichloromethane. The film was allowed to degrade in 40 °C buffer for 24 h, and the by-products were analysed using NMR. Similar results were obtained for homemade PCL-b-PLA diblock copolymer without any blended pure PLA homopolymer (10k-b-8k based on NMR analysis).

Crystal structures of BC–lipase and CA–lipase were taken from entries 3LIP and 1TCA in the protein data bank, respectively. Analysis of the proteinase K active site was carried out using entry 3PRK. Hydrophobic residues (grey) are defined as the following amino acids: alanine, glycine, valine, leucine, isoleucine, phenylalanine, methionine and proline. Aspartic acid and glutamic acid are defined as negative residues (red), whereas lysine, arginine and histidine are defined as positive residues (blue). The remaining residues are considered polar uncharged residues (purple). GPC on PCL–RHP–CA–lipase films (degraded in 37 °C buffer) was carried out following the same procedure as for BC–lipase-embedded films.

Confinement length scale affects degradation pathway

Degradation was run in a 1-ml and a 1-l container at 37 °C while shaking the container every few hours to demonstrate the effects of enzyme leaching and diffusion. PCL–RHP–BC–lipase degrades similarly in both volumes (≥95% degradation in 24 h), consistent with internal degradation and limited enzyme leaching.

Pure PCL films were placed in 1 l of buffer with an equivalent mass of total lipase as that present in the PCL–RHP–lipase films. Pure PCL films exhibited negligible degradation in 1 l of buffer over a week, whereas pure PCL films in 1 ml of buffer with the same enzyme mass lost ~80% mass in 1 day. This buffer volume dependence is expected, because the enzyme must diffuse to the plastic surface in order to hydrolyse the plastic.

To simulate experiments detailed in the previous literature for comparison[6,8], Tween 80 was mixed with purified lipase in a 1:1 mass ratio, lyophilized and resuspended in PCL–toluene to cast the films. In 1 l of buffer, films with Tween 80-embedded enzyme at the same enzyme loading as PCL–RHP–BC–lipase degraded by ~40% in 1 day and then stopped degrading (monitored over 1 week), whereas in 1 ml of buffer the small-molecule-embedded film degraded similarly to the RHP-embedded film (≥95% in 24 h). This reliance on buffer volume suggests that small-molecule surfactant-embedded enzyme experiments previously reported in the literature exhibit considerable leaching, and in large volumes this enzyme leaching prevents complete polymer degradation.

Kinetic analysis of BC–lipase in different environments with different substrates

Confined BC–lipase with PCL substrate. The slope of the degradation plot shown in Fig. 2a was used to estimate the degradation rate for confined lipase at 37 °C. Two different slopes were obtained (0–3 h and 3–5 h) and the rate changed at around 3 h. The turnover rate was determined by dividing the number of PCL bonds broken per second by the total number of lipase molecules in the film, assuming an average trimer PCL by-product based on the LC-MS by-product analysis.

Dissolved BC–lipase with PCL substrate. Pure PCL films (~5 mg each) were placed in 1 ml of buffer (37 °C) containing ~1 μg of lipase to mimic concentrations from degradation experiments of confined lipase. The turnover rate provided in section 'Design of enzyme–polymer blends for processive depolymerization' was determined by also assuming a trimer by-product, which may represent an upper bound, given that surface erosion can occur by random scission (larger oligomers generated per bond cleavage would serve to reduce the apparent turnover rate because more mass is lost per bond cleavage).

Dissolved and confined BC–lipase with small-molecule substrate. The same small-molecule assay was used to quantify the activity of dissolved and confined BC–lipase. 4-nitrophenyl butyrate was dissolved in buffer at each substrate concentration before running the assay to rule out interfacial effects of soluble lipase. The activity was quantified using ultraviolet–visible light spectroscopy to monitor the absorbance of the hydrolysed by-product at 410 nm over 10 min. The extinction coefficient for the by-product was estimated as 16,500 M^{-1} cm^{-1}. PRISM software was used to fit the activity as a function of substrate concentration to obtain V_{max}, the theoretical maximum reaction rate at saturated substrate concentration. V_{max} was converted to a turnover rate by converting the number of molecules per mass to number of molecules per lipase.

Dynamic interfacial-tension experiments to probe PCL–RHP–lipase interactions

The interfacial tension between a toluene and a water phase was used to probe the blends. A MilliQ water droplet was dispensed by a 1-ml syringe through a 1.27-mm-diameter needle and immersed in toluene. The droplet shape was captured by a CCD (charge-coupled device) camera every second and fitted by the Young–Laplace equation to obtain the interfacial tension. For each sample, the measurement was repeated three times and showed good consistency and reproducibility.

RHP and lipase were mixed in a 10:1 mass ratio and lyophilized to remove the aqueous solvent. A different ratio was used here compared to actual degradation studies, because 80:1 RHP:lipase resulted in unstable droplets due to high RHP interfacial activity, preventing accurate measurement. PCL was dissolved first in toluene at a concentration of 0.5 mg ml^{-1}. The PCL–toluene solution was then used to directly disperse RHP–lipase, giving a final concentration of 0.005 mg ml^{-1} for RHP and 0.0005 mg ml^{-1} for lipase in toluene. The concentration of each component was fixed across all groups. The water droplet was immersed in toluene after all three components (PCL, RHP and lipase) were dispersed in toluene.

To determine whether PCL alone could disperse lipase in toluene, fluorescently labelled lipase was dissolved in the water phase (0.75 mg ml^{-1} concentration), whereas PCL was dissolved in the toluene phase (0.5 mg ml^{-1}). The fluorescence intensity of both phases did not change over a 3-h period (data not shown), indicating the inability of PCL alone to disperse lipase in toluene via the water–toluene interface.

Melt processing, thermal treatment and operating temperature for programming degradation

PCL (10,000 g mol^{-1}) was first ground into a fine powder using a commercial grinder. RHP–lipase dried powder (1:1 mass ratio) was mixed with PCL powder, and all three components were again passed through the commercial grinder. The PCL–RHP–lipase powder was then placed in a single-screw benchtop extruder, with a rotating speed of 20 rpm and an extrusion temperature of 85 °C. Melt-extruded PCL–RHP–lipase filaments degrade with the same processive mechanism, as confirmed by GPC and LC-MS (data not shown).

For thermal treatment, PCL–RHP–lipase films were cast on microscope slides, placed on a hot plate at 80 °C for 5 min to ensure complete melting, and crystallized at the specified temperature for up to 3 days to ensure complete recrystallization.

To determine the dependence of degradation on the operating temperature, PCL–RHP–BC–lipase solution-cast films were placed in buffer at specified temperatures. For as-cast films, ramping the temperature from 20 °C to ~43 °C results in increased degradation rates. Further increases in temperature, however, result in degradation rate decreases. To rule out enzyme denaturation, the same small-molecule assay described in section 'Confinement affects degradation pathway: nanoscopic versus microscopic versus surface erosion' was employed at the given temperatures. Controls of only the 0.5 mM ester solution were run at each temperature to ensure that the ester was not self-hydrolysing over the given measurement time. The activity towards the small molecule increases greatly above 43 °C, ruling out denaturation as the cause for reduced PCL degradation at high temperatures.

RHPs with different compositions enable PLA depolymerization and regulation of embedded enzyme activity

The compositions of RHPs were screened to determine the effects of RHP–enzyme interactions on depolymerization by embedded enzymes. Three compositions were chosen on the basis of segmental hydrophobicity, which was determined by simulating RHP sequences. Briefly, RHP sequences were generated using the program Compositional Drift[43]. The hydrophile–lipophile balance (HLB) value was used to evaluate the solubility of monomer side-chains through group contribution theory. Using the equation $HLB = 7 + \sum_i n_i HLB_i$, where n_i is the number of the ith chemical group in the molecule with corresponding value HLB_i. The HLB value for each monomer side-chain was estimated as: HLB(MMA) = 8.45, HLB(EHMA) = 5.12, HLB(OEGMA) = 11.4 and HLB(SPMA) = 18.5. A lower HLB value denotes higher hydrophobicity and a higher value means greater hydrophilicity. A Python program was created to continuously calculate the average segmental HLB values for a window sliding from the alpha to the omega ends of the simulated RHP chains. The window advanced by one monomer each time. We used a span containing odd numbers of monomers and assigned the average HLB value of that span to its middle monomer. A window size of 9 was used as an intermediate segmental region size.

Hydropathy plots were generated to visualize randomly sampled sequences for each RHP composition and window size. An HLB threshold of 9 was set to distinguish hydrophobic and hydrophilic segments. The sequences were then averaged both across positions along the chain as well as across all 15,000 sequences in a simulated batch to make batch-to-batch comparisons on the average segmental (window) hydrophobicity.

Similar tensiometry experiments as those outlined in section 'Dynamic interfacial-tension experiments to probe PCL–RHP–lipase interactions' were carried out using RHP (0.005 mg ml^{-1})–proteinase K (0.0025 mg ml^{-1}), PLA and dichloromethane. PLA showed little interfacial activity. For the 20:50 MMA:EHMA RHP, addition of PLA measurably reduced the interfacial activity of the RHP. The 50:20 MMA:EHMA RHP had similar interfacial activity with and without PLA.

Depolymerization in ASTM composts and tap water

PCL–RHP–BC–lipase films were placed in tap water or a custom-made compost setup mimicking industrial compost conditions. For water, films were submerged in 100 ml of tap water from a sink, and degradation proceeded identically to that in buffer over 24 h (>95%) at the specified temperature. Soil was purchased from a local composting facility. The total dry organic weight of the soil was determined by leaving a known soil mass in an oven set to 110 °C overnight, and then weighing the remaining material mass. Water was added to the soil to achieve a total moisture content of 50% or 60%, consistent with ASTM standards. For PCL–RHP–BC–lipase, up to 40% mass loss and 70% mass loss was observed after 2 and 4 days, respectively, in the compost setup at 40 °C. For PLA–RHP–proteinase K, ~34% mass loss occurred for 40 kDa PLA and ~8% mass loss occurred for 85–160 kDa PLA after 5 days in a 50 °C soil compost.

Oxidative enzymes embedded in polyolefins

Manganese peroxidase from white rot fungus and laccase from *Trametes versicolor* were purchased from Sigma Aldrich and used as purchased. RHP (50:20 MMA:EHMA) was mixed with either enzyme in a 4:1 ratio. Both enzymes were embedded in polyethylene (weight-average molecular weight, M_w = 35 kDa) or polystyrene (M_n = 260 kDa). For polyethylene, enzymes were embedded by solution-casting from a 5 wt% solution in toluene or melt-pressing at 95 °C from polyethylene powder. For polystyrene, enzymes were embedded by resuspending directly in a 10 wt% polystyrene in dichloromethane solution. Enzymes were embedded with and without mediators (Tween 80 for manganese peroxidase and hydroxybenzotriazole for laccase). The films were then placed in 30 °C or 60 °C malonate buffer (pH 4.5) for up to two weeks. After drying the films, infrared spectroscopy and GPC were used, and no changes were observable for any enzyme–polyolefin system.

To confirm that enzymes were still active after embedding inside polyolefins, the films were submerged in a 1 mM solution of the small molecule 2,2′-azino-bis(3-ethylbenzothiazoline-6-sulfonic acid) diammonium salt (ABTS) in malonate buffer. The solution turned dark blue for both manganese peroxidase and laccase, demonstrating that the embedded enzymes retained a high portion of activity. Tensiometry tests were carried out using RHP–manganese peroxidase or RHP–laccase with or without PS in toluene in the same setup and concentrations outlined for PCL–lipase. RHP–enzyme clusters with both enzymes achieved the same final interfacial tension with or without PS present, and no lag phase or change in final interfacial tension, suggesting that the PS chains do not strongly interact with the enzymes.

Data availability

All data are available in the main text or the Supplementary Information. Additional requests can be made to the corresponding author.

40. Bornscheuer, U. et al. Lipase of pseudomonas-cepacia for biotechnological purposes – purification, crystallization and characterization. *Biochim. Biophys. Acta Gen. Subj.* **1201**, 55–60 (1994).
41. Wurm, A. et al. Crystallization and homogeneous nucleation kinetics of poly(epsilon-caprolactone) (PCL) with different molar masses. *Macromolecules* **45**, 3816–3828 (2012).
42. Ajioka, M., Suizu, H., Higuchi, C. & Kashima, T. Aliphatic polyesters and their copolymers synthesized through direct condensation polymerization. *Polym. Degrad. Stabil.* **59**, 137–143 (1998).
43. Smith, A. A. A., Hall, A., Wu, V. & Xu, T. Practical prediction of heteropolymer composition and drift. *ACS Macro Lett.* **8**, 36–40 (2019).

Acknowledgements This work was primarily supported by the US Department of Energy, Office of Science, Office of Basic Energy Sciences, Materials Sciences and Engineering Division (DOE-BES-MSE) under contract DE-AC02-05-CH11231, through the Organic–Inorganic Nanocomposites KC3104 programme (enzyme–plastic composite design and degradation mechanism; C.D., L.M., A.H., I.J., R.O.R., T.X.). Y.J. and T.P.R. acknowledge support from DOE-BES-MSE under the same contract number, through the Adaptive Interfacial Assemblies Towards Structuring Liquids KCTR16 programme (tensiometry studies on RHP/enzyme/polymer complexation). C.D.S. acknowledges Laboratory Directed Research and Development funding from Berkeley Lab (integration with organic waste infrastructure). The US Department of Defense, Army Research Office supported Z.R. (lipase stabilization) under contract W911NF-13-1-0232. C.D. was partially supported by a National Defense Science and Engineering Graduate (NDSEG) Fellowship (Bioremediation). T.X. also acknowledges support from a Bakar Fellowship at University of California Berkeley (compost tests). Scattering studies at the Advanced Light Source were supported by the US Department of Energy, Office of Science, Office of Basic Energy Science under contract DE-AC02-05CH11231.

Author contributions T.X. conceived the idea and guided the project. C.D. and T.X. analysed degradation rate and by-product experiments, material characterization experiments, and determined the different enzyme mechanisms. C.D., Y.J., T.P.R. and T.X. analysed interfacial-tension data. C.D., P.K. and T.X. analysed the diblock degradation experiments. J.K. and R.O.R. analysed mechanical properties. P.K., Z.R. and A.H. synthesized and characterized the RHPs. I.J. analysed RHPs and enzyme surfaces and repeated the analysis of the degradation results. L.M. performed electron microscopy experiments. A.H. carried out repolymerization experiments. K.Z. and T.L. assisted with degradation-rate quantification and enzyme active-site analysis. C.D.S. provided insights on integration with organic-waste infrastructure.

Competing interests T.X., C.D. and J.K. have filed a PCT patent application. A.H. is the founder and CEO of Intropic Materials.

Additional information
Correspondence and requests for materials should be addressed to T.X.
Peer review information *Nature* thanks Jayati Ray Dutta, Mattheos Koffas and the other, anonymous, reviewer(s) for their contribution to the peer review of this work.
Reprints and permissions information is available at http://www.nature.com/reprints.

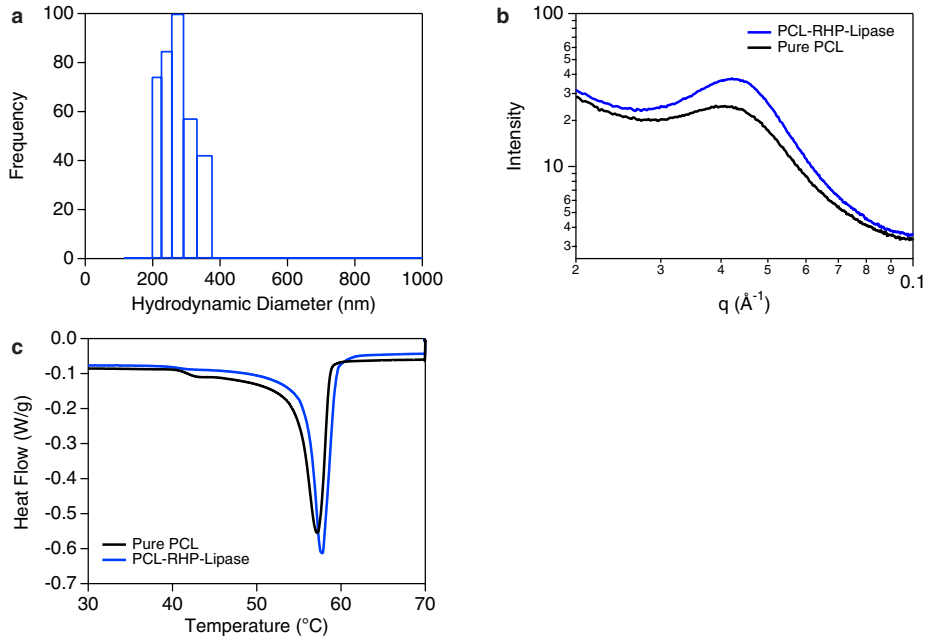

Extended Data Fig. 1 | Characterization of enzyme-embedded PCL. a, DLS results for RHP and purified BC–lipase in toluene (the solvent used to cast PCL) with an average hydrodynamic diameter of 285 nm ± 35 nm (n = 5) (the error indicates standard deviation). **b**, DSC results for PCL and PCL–RHP–BC-lipase as-cast films. **c**, SAXS curves of PCL and PCL–RHP–BC–lipase as-cast films.

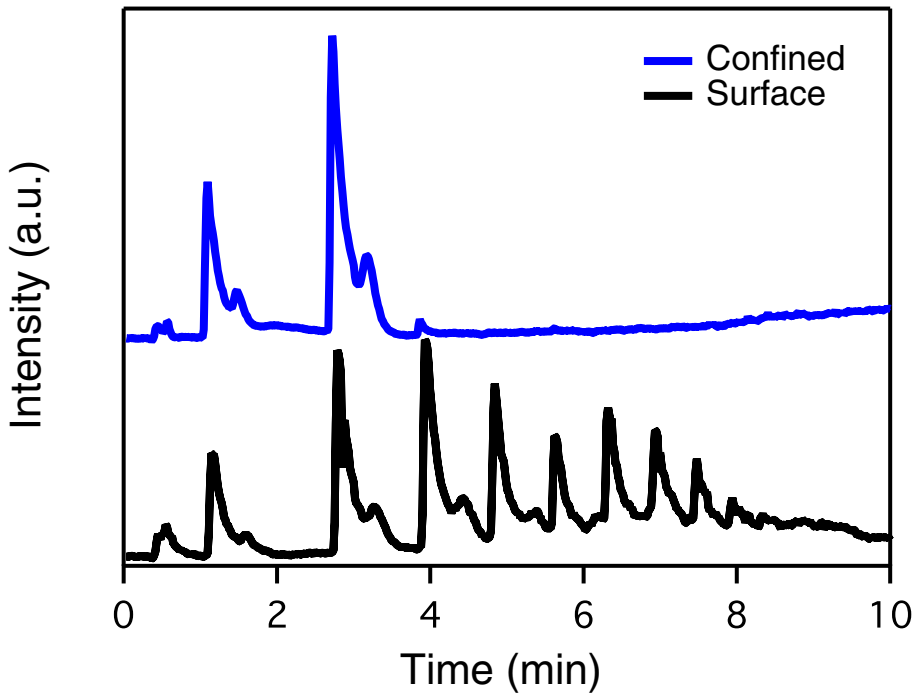

Extended Data Fig. 2 | PCL–RHP–BC–lipase by-product analysis. Liquid chromatogram of the degradation by-products for degradation by confined and dissolved (surface erosion) BC–lipase.

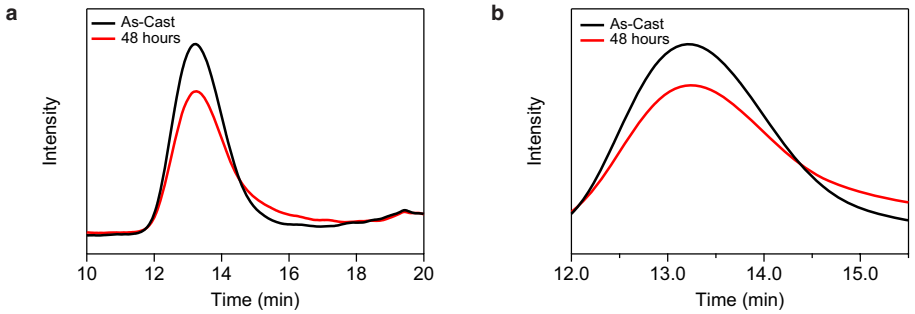

Extended Data Fig. 3 | Degradation by confined CA–lipase with shallow active site. a, GPC curve of the degradation of PCL–RHP–CA–lipase, showing a shift and broadening of the main peak, indicative of random chain scission. **b**, Zoomed-in version of **a** illustrating the peak shift and broadening.

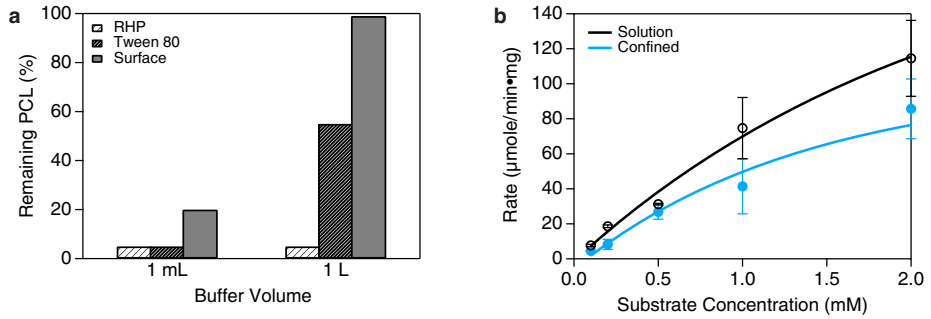

Extended Data Fig. 4 | Enzyme environment dictates biocatalytic reaction kinetics. a, PCL degradation by BC–lipase dissolved in solution (surface), nanoscopically embedded in PCL with RHP, and embedded with Tween 80, a small-molecule surfactant, as microparticles. **b**, Hydrolysis of 4-nitrophenyl butyrate, a small-molecule ester, by BC–lipase in solution or confined in PCL (error bars represent one standard deviation; $n \geq 3$).

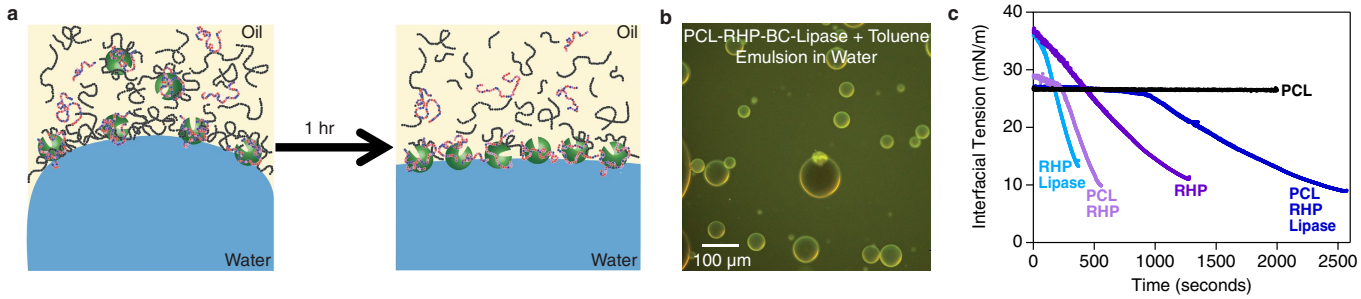

Extended Data Fig. 5 | Model interfacial-tension experiment to explain intermolecular interactions among enzyme, protectant and matrix. **a**–**c**, When all three components are initially mixed in toluene (**a**, left) and then a water interface is introduced (**a**, right), RHP–lipase complexes immediately interact with PCL at the interface, as shown by the fluorescence microscopy image taken ~20 s after shaking the vial to produce an emulsion (**b**) and the long delay time in interfacial-tension reduction that is seen only for PCL–RHP–lipase (**c**).

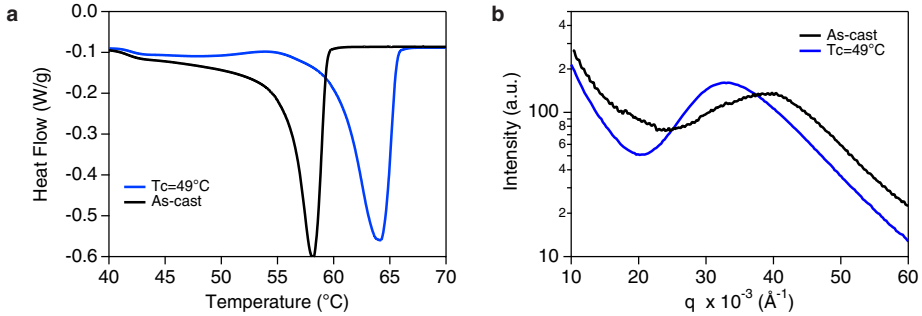

Extended Data Fig. 6 | Characterization of semi-crystalline properties of melt-processed PCL–RHP–BC–lipase. a, DSC curves of PCL–RHP–BC–lipase with different recrystallization conditions (the film with recrystallization temperature T_c = 49 °C has a crystallinity of 41% ± 1.2% compared to 39% ± 1.8% for the as-cast film). The increase in melting temperature from ~58 °C to ~64 °C indicates a substantial thickening in crystalline lamellae for T_c = 49 °C films, which was confirmed by SAXS. **b**, SAXS profiles of as-cast and T_c = 49 °C films of PCL–RHP–BC–lipase. The increase of long periods (shift to lower q), combined with the negligible difference in the bulk per cent crystallinity according to DSC data, confirms a thickening in crystalline lamellae after crystallizing at T_c = 49 °C.

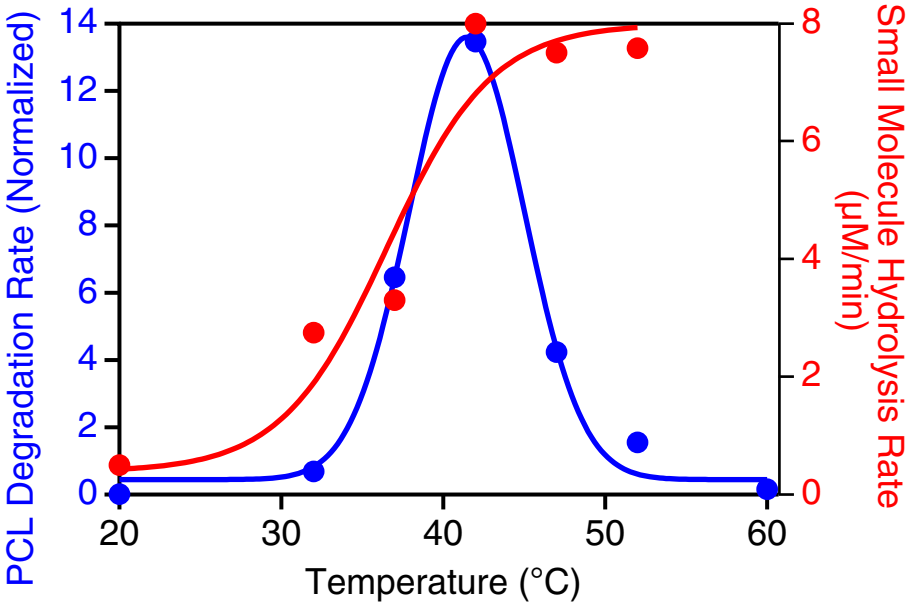

Extended Data Fig. 7 | Confirming enzyme does not denature at high temperatures. Small-molecule ester hydrolysis by embedded BC–lipase as a function of temperature (red), overlaid with the PCL–RHP–BC–lipase degradation rate. The small-molecule activity remained high at 60 °C but was not quantified because the film shrivelled owing to melting, and thus was much thicker than films at lower temperatures, making quantification incomparable to all other temperatures.

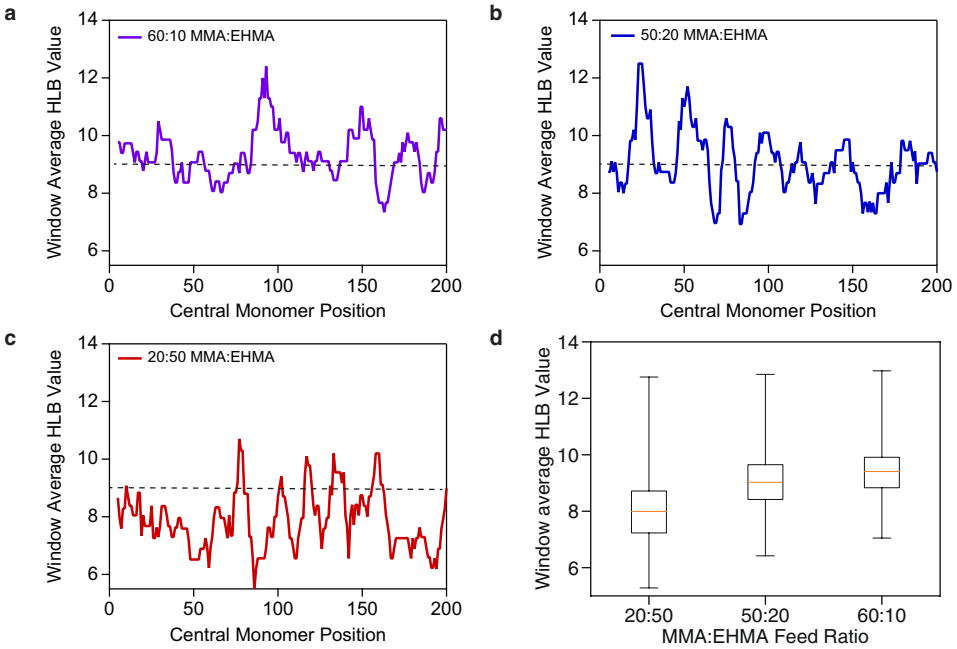

Extended Data Fig. 8 | Quantifying segmental hydrophobicity of different RHPs. a, Hydropathy plots for RHPs with 60:10 MMA:EHMA composition. **b**, Hydropathy plots for RHPs with 50:20 MMA:EHMA composition. **c**, Hydropathy plots for RHPs with 20:50 MMA:EHMA composition. **d**, Average segmental HLB value for each RHP composition. Error bars indicate standard deviation, $n \geq 3$.

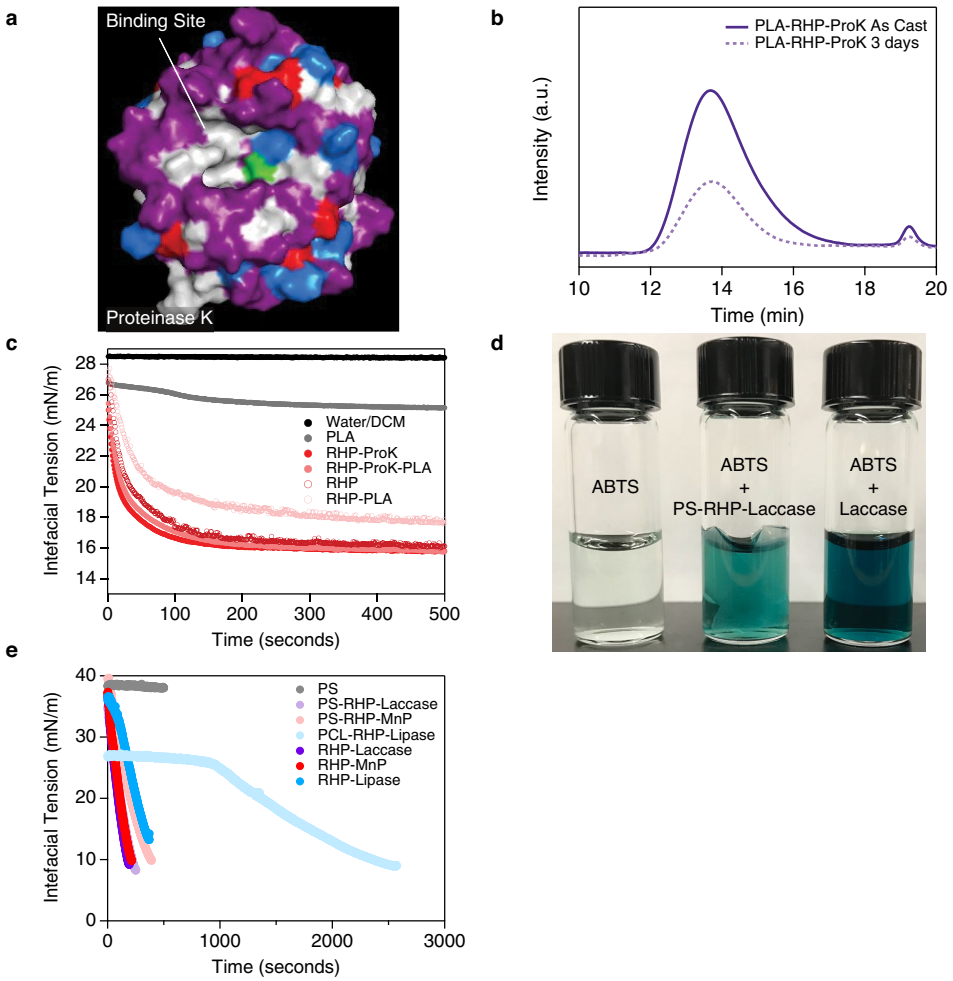

Extended Data Fig. 9 | Characterizing embedded enzymes for more commercially relevant plastics. a, Crystal structure of proteinase K with the same colour-coding scheme as that used for lipases in the main text (Fig. 3). **b**, GPC curve of PLA–RHP–proteinase K ('ProK") as cast and after depolymerizing in buffer; **c**, Interfacial-tensiometry experiment results for a DCM–water interface with PLA, RHP and proteinase K in the DCM phase. **d**, Photograph of ABTS small-molecule assay in malonate buffer after ~10 min, demonstrating that laccase embedded in polystyrene (PS) retains the ability to oxidize a small molecule. Similar results were found for manganese peroxidase and for both enzymes embedded in polyethylene. **e**, Interfacial-tensiometry experiment results for a toluene–water interface with PS, RHP and either laccase or manganese peroxidase ('MnP') in the toluene phase.

Extended Data Table 1 | Summary of all polymer–enzyme blends employed in the study

Sample	Enzyme	RHP (MMA:EHMA:OEGMA:SPMA)	RHP MW (kDa)	RHP PDI	RHP:Enzyme (mass ratio)	Polymer Host	Polymer:RHP:Enzyme (%)
p-BC1*	Purified BC-lipase	50:20:25:5	69	1.55	80:1	PCL 80 kDa	98.6:1.4:0.017
p-BC2†	Purified BC-lipase	50:20:25:5	25	1.6	80:1	PCL 80 kDa	98.6:1.4:0.017
p-BC3	Purified BC-lipase	Tween 80	N/A	N/A	1:1‡	PCL 80 kDa	99.9:0.017:0.017
p-BC4	Purified BC lipase	50:20:25:5	69	1.55	80:1	PCL/PLLA Blend (75/25 and 50/50 by wt)	98.6:1.4:0.017
p-BC5	Purified BC lipase	50:20:25:5	69	1.55	80:1	PCL-b-PLLA + pure PLLA (9/4 by wt)	98.6:1.4:0.017
p-BC6	Purified BC lipase	50:20:25:5	69	1.55	1:1	PCL 10 kDa	99.9:0.06:0.06
p-BC7	Purified BC-lipase	60:10:25:5	18.5	1.45	80:1	PCL 80 kDa	98.6:1.4:0.017
p-BC8	Purified BC-lipase	20:50:25:5	25.6	1.31	80:1	PCL 80 kDa	98.6:1.4:0.017
BC1	BC-lipase blend	50:20:25:5	69	1.55	2:1	PCL 80 kDa	94.9:3.4:1.7
CA1	CA-lipase blend	50:20:25:5	69	1.55	2:1	PCL 80 kDa	94.9:3.4:1.7
ProK1	Proteinase K	50:20:25:5	69	1.55	2:1	PLLA 85-160 kDa	95.5:3.0:1.5
ProK2	Proteinase K	60:10:25:5	18.5	1.45	2:1	PLLA 85-160 kDa	95.5:3.0:1.5
ProK3	Proteinase K	20:50:25:5	25.6	1.31	2:1	PLLA 85-160 kDa	95.5:3.0:1.5

*p-BC1 is the sample referred to as PCL–RHP–BC–lipase in the text.
†p-BC2 was tested, but no degradation data are provided in the text.
‡Conditions simulate experiments from previous literature.